Peptide Amphiphiles and their use in Supramolecular Chemistry

Versluis, F.

Chapter 2

Power Struggles between Oligopeptides and Cyclodextrin Vesicles

Stimulus responsive supramolecular assemblies were constructed by decorating the surface of *β*-cyclodextrin vesicles (CDVs) with *β*-sheet forming oligopeptides. Three octapeptides were used to coat the CDVs: adamantane-(leu-glu)$_4$ **(1)**, adamantane-PEG$_4$-(leu-glu)$_4$ **(2)** and (adamantane-PEG$_4$)$_2$-(leu-glu)$_4$ **(3)**. The adamantane moiety ensured the binding of the peptides at the surface of the CDVs. At pH 7.2, all the peptides typically adopt a random coil secondary structure. Upon acidification to ~pH 5 however, a transition to well-defined *β*-sheet structures was observed. The pH at which this transition occurred was found to be influenced by the PEG$_4$-spacer and the number of adamantane residues conjugated to the octapeptide hybrids. Furthermore, by raising the pH back to 7.2, the β-sheet structures were dissolved, showing that the transitions in secondary structures of the peptides were reversible. The structural rearrangement of the peptide backbone to accommodate β-sheet formation was found to induce a morphological transition of the entire assembly. For the peptide **(1)**-CDV assembly a reversible transition to fiber like structures was observed, whereas bundles of aggregated fibers were present in the peptide **(2)**-CDV assembly. Upon addition of peptide **(3)**, the structural integrity of the CDVs was lost. The peptide **(1)**-CDV assembly shows promise as a nano-scale switching device which releases its contents due to the pH-induced vesicle-to-fiber transition. The amount of released cargo could be controlled as a function of pH and peptide concentration.

This work is published: F. Versluis, J. Voskuhl, M. C. A. Stewart, J. B. Bultema, S. Kehr, B. J. Ravoo and A. Kros, *Soft Matter*, 2012, **8**, 8770-8777.

F. Versluis, I. Tomatsu, S. Kehr, C. Fregonese, A. W. J. W. Tepper, M. C. A. Stewart, B. J. Ravoo, R. I. Koning and A. Kros, *J. Am. Chem. Soc*, 2009, **131**, 13186-13187.

Introduction

The field of supramolecular chemistry involves the design and synthesis of compounds which are able to form structures with a high degree of internal order, so called suprastructures. Dynamic and responsive architectures have recently received a lot of interest as they have possible applications in materials science and medicine.[1-3] The most viable way to obtain these structures is self-assembly of the molecular components, which can be driven by a variety of noncovalent interactions such as hydrogen bonding,[4, 5] electrostatic[6] and hydrophobic interactions[7] and metal complexation.[8, 9] By carefully designing the constituents of the suprastructure, the noncovalent forces can be balanced in such a way that accurate placement of individual atoms in three dimensions can be obtained. Therefore, self-assembly is a potent strategy for the design and synthesis of functional materials whose characteristics can be tuned for a wide range of applications.[10-12] Consequently, it is not surprising that recent years have witnessed an overwhelming number of new functional materials such as hydrogels,[13-15] metal organized frameworks (MOF)[16] as well as vesicles[17] and liposomes.[18] Furthermore peptides are versatile building block for the construction of suprastructures.[19] Recently, several groups used peptides to construct suprastructures such as fibers and rods which were used in biological and medicinal applications.[20-22]

The formation of vesicles and liposomes is mainly driven by hydrophobic interactions and they have been found interesting candidates for the transport of active agents such as drugs,[23] nanoparticles[24] and dyes.[25] These structures are composed of a bilayer membrane that entraps the aqueous interior, for which charged or neutral phospholipids are typically used. However, it is well known from the literature that it is also viable to form vesicles consisting of non-lipid materials such as carbohydrates,[26] peptides[27] and blockcopolymers.[28, 29] In 2000, Ravoo and Darcy were the first to describe the formation of vesicles by amphiphilic cyclodextrins.[30] Cyclodextrins are cyclic oligosaccharides (6-8 repeating glucose units) and are increasingly used in areas such as medicine[31, 32] material sciences[33] and catalysis.[34] They have become important partly due to their high availability, non toxicity and low cost, but more importantly, they are donut shaped structures which enable the formation of stable inclusion complexes in aqueous media with hydrophobic guest

molecules such as adamantane-, ferrocene- and bulky aromatic derivatives (K_a = 1.5-3.2 x 10^5 M^{-1}).[35]

Recent studies have shown that vesicles of amphiphilic cyclodextrins could be decorated with different guest molecules such as adamantane functionalized peptides[36, 37] and carbohydrates.[38] Furthermore it was shown that light responsive azobenzene guest molecules could be introduced and released by an external light stimulus from the vesicle surface, leading to an aggregation and deaggreagtion process.[39] With the help of an azobenzene-spermine conjugate it was also possible to bind and release oligonucleotides from the cyclodextrin vesicle surface.[40]

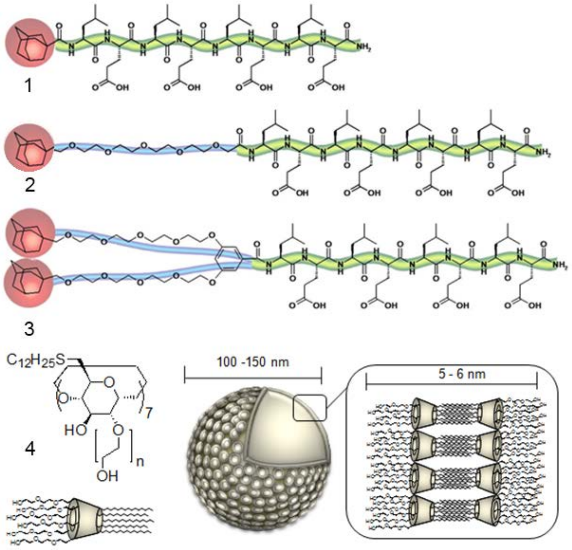

Scheme 1. *Chemical structures of the adamantylated oligopeptides **(1)**, **(2)** and **(3)**. These peptides were added to vesicles composed of an amphiphilic β-cyclodextrin derivative **(4)**.*

In the present study, vesicles composed purely of amphiphilic *β*-cyclodextrin **(4)**, were used, these were subsequently decorated with oligopeptides **(Scheme 1)**. The *oligo*peptides used in this study consist of the sequence (leu-glu)$_4$, and were covalently coupled to adamantane to ensure efficient binding to the CDVs. The peptides consist of alternating hydrophobic (leucine) and hydrophilic (glutamic acid) amino acid residues. Polypeptides with this type of sequence have a tendency to form *β*-sheet domains.[41] However, the short oligopeptides used in this study, are typically unstructured upon dispersion in aqueous media. In order to be able to form *β*-sheet structures with this short peptide, the local concentration of the peptide needs to be

sufficiently high. This can be achieved by attaching the peptide to a scaffold, which in our case is the CDV. Hence, with this oligopeptide *β*-sheet structures could be formed at the surface of the *β*-cyclodextrin vesicles.

In this study, three different oligopeptides **(Scheme 1)** were used which can be denoted as ada-(leu-glu)$_4$ **(1)**, ada-PEG$_4$-(leu-glu)$_4$ **(2)** and (ada-PEG$_4$)$_2$-(leu-glu)$_4$. Peptide amphiphile **(1)** is the most simple, containing just the oligopeptide, which was covalently linked to adamantane. In peptide **(2)**, a PEG$_4$ spacer was incorporated between peptide and adamantane segment. In peptide **(3)**, two ada-PEG$_4$ segments were coupled to the oligopeptide. Our goal was to form β-sheet regions at the surface of cyclodextrin vesicles. Furthermore, the overall morphology of the assemblies and the changes therein upon β-sheet formation was studied. In these peptide-CDV assemblies, three orthogonal noncovalent interactions were combined: 1) hydrophobic interactions between alkylated cyclodextrins, resulting in the formation of bilayer vesicles, 2) the inclusion complex formation of *β*-cyclodextrin and adamantane, which is based on size specific hydrophobic interactions and 3) intermolecular hydrogen bonding between adjacent peptide strands. The deliberate orchestration of these forces opens up the opportunity to reversibly form highly defined *β*-sheet structures at the surface of CDVs.

Results and discussion

Binding of peptides to *β*-cyclodextrin

To determine the binding constants and ratios of inclusion complex formation between the peptides and the *β*-cyclodextrin cavity, isothermal titration calorimetry experiments were conducted. The results show strong binding affinities between the peptides and *β*-cyclodextrin (**Figure 1** and **Table 1**), which is a clear indication that the peptide and spacer do not affect inclusion complex formation between adamantane and *β*-cyclodextrin. The expected 1:1 stoichiometric binding between the peptide and *β*-cyclodextrin was observed for all three peptides. Furthermore, the complexation of the adamantane moieties is mainly enthalpy ($\Delta H < 0$) driven. This could be explained by the release of water molecules from the cyclodextrin cavity, as well as the docking of the hydrophobic adamantane residue into the cyclodextrin cavity, which has been described by several groups for cavity-like host molecules.[42, 43]

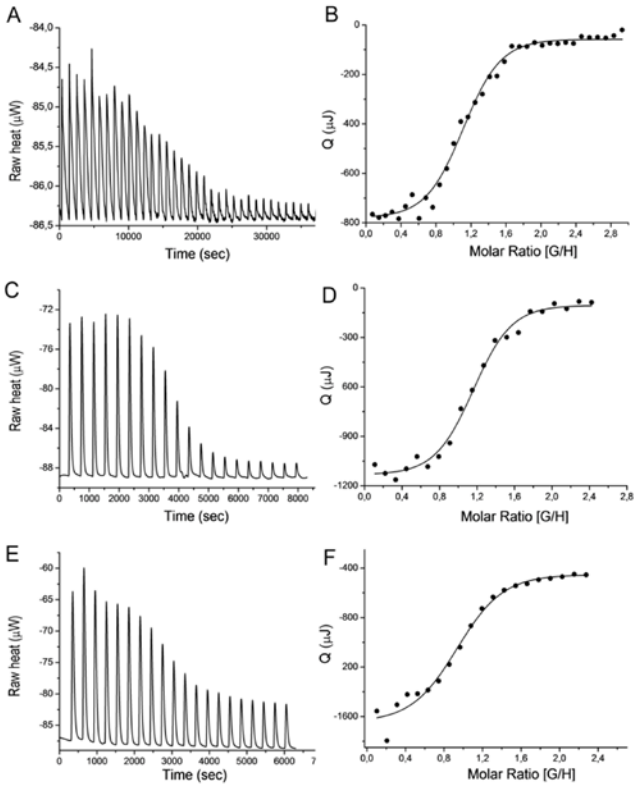

Figure 1. *ITC measurements for the addition of oligopeptides to β-cyclodextrin. For peptide **(1)** A) raw heat, B) Molar ratio of guest and host, peptide **(2)** C) raw heat, D) molar ratio of guest and host and peptide **(3)** E) Raw heat, F) molar ratio of guest and host.*

The binding energy calculations were based on the assumption that adamantane forms a 1:1 host-guest complex with a *β*-CD and the two adamantane moieties of peptide **(3)** were seen as independent guests for the cyclodextrin cavities. Therefore it can be concluded that when peptides **(1)**, **(2)** or **(3)** are added to a solution of CDVs, they will bind to their surface. Furthermore, the divalent binding of **(3)** results in a higer binding constant on the CD-vesicles surface, which is in the order of 10^7 M^{-1},[44] compared to 10^4 M^{-1} for the monovalent binding of peptides **(1)** and **(2)**.

Table 1. *Thermodynamic parameters of the complexation between peptides **(1)**, **(2)** and **(3)** and β-CD as obtained from ITC measurements. All the thermodynamic parameters are represented per adamantane moiety.*

guest	host	ΔH kJ/mol	ΔG kJ/mol	ΔS (kJ/mol)	K (M^{-1})
1	*β*-CD	-21,60	-25.71	13.88	3.47×10^4
2	*β*-CD	-22.11	-27.10	16.74	5.62×10^4
3	*β*-CD	-23.31	-26.77	11.61	4.93×10^4

Peptide secondary structure

The secondary structure of the peptides **(1)**, **(2)** and **(3)** as influenced by scaffolding to CDVs and in response to pH were examined using circular dichroism spectroscopy. When the peptides were dispersed in PBS, they all adopted an unordered random coil secondary structure. Upon lowering the pH, a transition in the structure was observed to a mixture of random coil and *β*-sheet **(Appendix, Figure S1)**. When the peptides were mixed with the *β*-cyclodextrin vesicles (with a peptide: *β*-cyclodextrin ratio of 1:2) they also show no clear structure at pH 7.3, due to electrostatic repulsion between the peptide strands **(Figure 2A)**. However, acidification of the mixed assemblies to approximately pH 5, led to a random coil to β-sheet structure transition **(Figure 2B)**. This finding is in line with the common observation that oligopeptides which are attached to a scaffold can show a significantly altered behavior to free peptides in solution.[41] By confining the peptide moieties to the surface of a self-assembled structure, the local peptide concentration is raised, which aids the process of the formation of a well-defined secondary structure. Also, the freedom of motion of the

peptides is limited, which can further stabilize the structure. Typically, long peptides are required to obtain structures with a high degree of internal order, however in our system a short octapeptide was able to fold into well defined *β*-sheet structures. The pH at which this transition occurred was different for the three peptides. Conversion to a *β*-sheet structure for peptide **(1)** was observed at pH 5.0, for peptide **(2)** at pH 5.3 and for peptide **(3)** at pH 5.6.

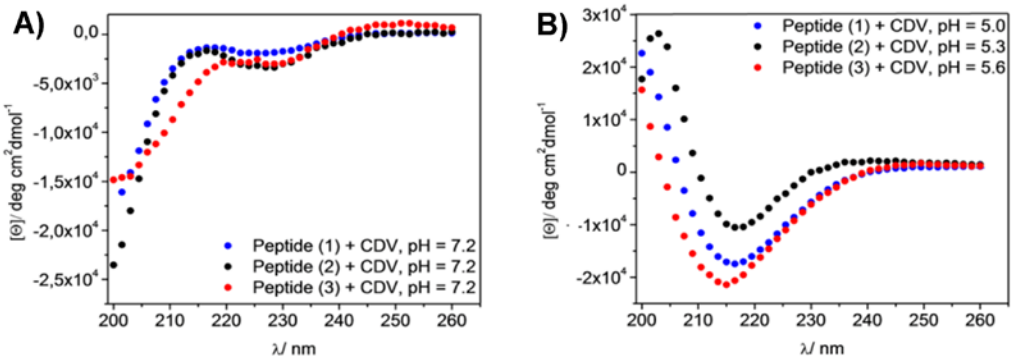

Figure 2. A) Peptide **(1)**, **(2)** and **(3)** mixed with 0.5 mM *β*-CD vesicles at 50 mol% at pH 7.2 B). Peptide **(1)** , **(2)** and **(3)** mixed with 0.5 mM *β*-CD vesicles at 50 mol% at pH 5.0, pH 5.3 and pH 5.6 respectively.

The reversibility of the observed transitions from random coil to *β*-sheet was examined by measuring the CD signal at alternating high and low pH. It was observed that the transition from random coil to *β*-sheet structure were reversible for all peptides, as can be observed in **Figure 3**. Furthermore, peptide **(3)** has the strongest CD signal followed by peptide **(1)** and finally peptide **(2)**. This, in turn indicates that peptide **(3)** forms *β*-sheet domains the most efficiently.

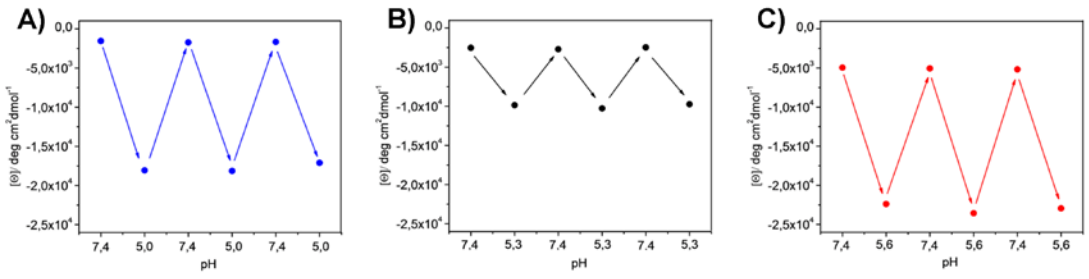

Figure 3. *Switching between random coil and β-sheet formation upon changing the pH between 7.4 and ~5 of assemblies containing 0.5 mM CDVs and A) 50 mol% peptide* ***(1),*** *B) 50 mol% peptide* ***(2)*** *and C) 50 mol% peptide* ***(3).***

So far all studies were performed in a 1:2 ratio (adamantane to cyclodextrin) ensuring that all amphiphilic cyclodextrins at the outer surface of the vesicles formed a complex with the adamantane modified octapeptide. Now, the influence of the oligopeptide: *β*-cyclodextrin ratio on the *β*-sheet structure formation was of interest. For each peptide the ratio was varied from 0.1 to 1.0 equivalent of peptide molecules relative to the number of *β*-cyclodextrin amphiphiles and the resulting circular dichroism signal was measured for each sample. The circular dichroism signal at 215 nm for all samples is displayed in **Figure 4**. First of all, all peptides show a maximum CD signal around 0.5 equivalents of peptide, which implies for peptide **(1)** and **(2)** that *β*-sheet formation is most efficient when the surface of the CDVs is completely covered, taking into account that around 50% of the *β*-cyclodextrin molecules are in the outer leaflets of the CDVs and are therefore available for inclusion complex formation **(Figure 4)**. It was anticipated that peptide **(3)**, as it bears two adamantane moieties, would reach the optimum CD signal at 0.25 eq. peptide, but surprisingly this was not observed. An explanation for this phenomenon can be found by a change in the overall morphology of the assembly (vide infra). It is also of interest to observe a difference in intensity of the CD signal between the three adamantylated peptides. The most intense CD signal belongs to peptide **(3)**, which might be due to the increased stabilization of the peptide-CDV complex that the additional adamantane gives, which influences the folding of the peptide into the well-defined *β*-structure. The lowest CD intensity belongs to peptide **(2)**. The only difference between peptide **(1)** and (**2)** is the short PEG spacer, which induces less efficient *β*-sheet formation. It can be hypothesized that the additional spacer between the adamantane and oligopeptide segments decreases the stabilizing effect that the binding of the peptide to the CDVs has. Through the flexible spacer, the oligopeptide acquires additional translational freedom, which destabilizes the *β*-sheet structures.

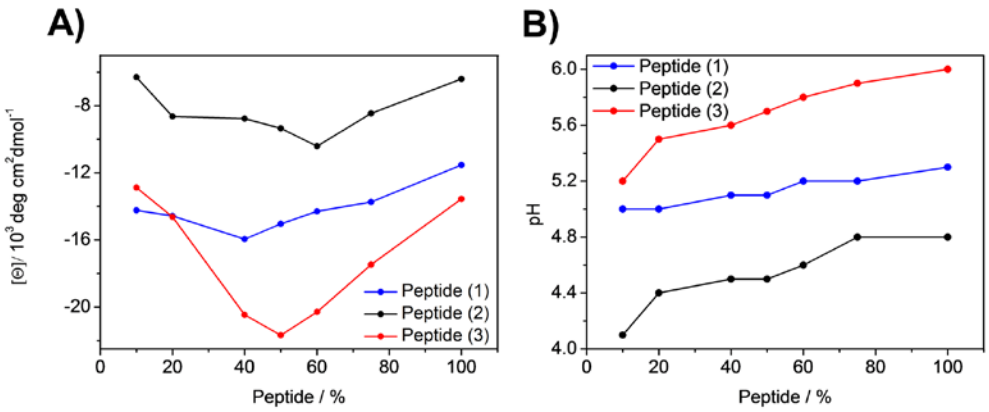

Figure 4. *A) The ellipticity at 215 nm was measured for assemblies composed of 0.5 mM CDVs and various concentrations of peptide* ***(1)***, ***(2)*** *and* ***(3)***. *B) In samples containing 0.5 mM CDVs, the pH at which the transition from random coil to a β-sheet structure occurs, depending on the peptide density at the CD surface is displayed for various concentrations of peptide* ***(1)***, ***(2)*** *and* ***(3)***.

Further investigations were aimed at unraveling the pH at which the transition from random coil to *β*-sheet structures occurs for the different peptide and at different peptide concentrations. This was determined by the stepwise lowering of the pH of the peptide-CDV solution and measuring the ellipticity at 215 nm at each pH-step **(Figure 4B)**. The maximum CD intensity at this wavelength indicates a maximum in the number of peptide molecules that are in *β*-sheet conformation. First of all, at higher peptide concentrations, a higher pH is sufficient to achieve the CD signal with maximum intensity and this trend was observed for all three peptides. This is probably due to the fact that as the peptide concentration increases, the *β*-sheet domains at the CDV surface become larger, and as they grow larger, the edges of these domains become less pronounced, as compared to the total area of the sheet. These less stable edges of the *β*-sheet domains can only be stabilized by reducing the negative charge of the glutamic acid residues present in the oligopeptide and therefore the samples with low peptide concentrations require a lower pH to make the transition between random coil and *β*-sheet structures. Secondly, a difference in transition pH is observed between the three peptides. A higher pH is sufficient for the transition for peptide **(2)** than peptide **(1)**. Because of the additional PEG spacer present in peptide **(2)**, it extends further from the CDV surface. Therefore, the peptide strand might be able to interact with peptide strands located at adjacent vesicles. Support for this hypothesis

can be obtained by studying the overall morphology of the assembly, which will be discussed in the next section. For peptide **(3)**, an even higher pH is sufficient to form β-sheet domains. This is thought to be due to the additional adamantane present in this peptide hybrid. The divalent binding to the CDVs enhances the stability significantly, thereby aiding the folding of the peptide into the well defined β-sheet structure.

Morphology of the assemblies

CDV + peptide (1)

In the following sections the morphology of the assemblies formed by the CDVs and peptides **(1)**, **(2)** and **(3)** as a function of pH is addressed, focusing on the morphological transitions associated with the secondary structure transitions of the peptides. First, the assembly containing CDVs and peptide **(1)** is examined. Upon addition of the oligopeptide **(1)** at pH 7.4, no changes in morphology or size were observed and the 100 nm spherical vesicles, typical of CDVs, were present **(Figure 5)**. However, upon acidification to pH 5, the predominant structures were thin fiber-like aggregates with a thickness of around 8 nm and a length up to several hundred nm. Upon hydrogen bonding between the peptide strands the *β*-cyclodextrin molecules in the CDVs are forced to reorganize to accommodate a fiber-like structure. The pH was raised again to 7.4, to examine the effect of disassembling the *β*-sheet, resulting in a random coil secondary structure. As is clear from **Figure 5D**, the vesicular morphology of the assembly reappeared. This shows that both the transition from random coil to *β*-sheet as well as the resulting rearrangement from spheres to fibers is reversible and fast.

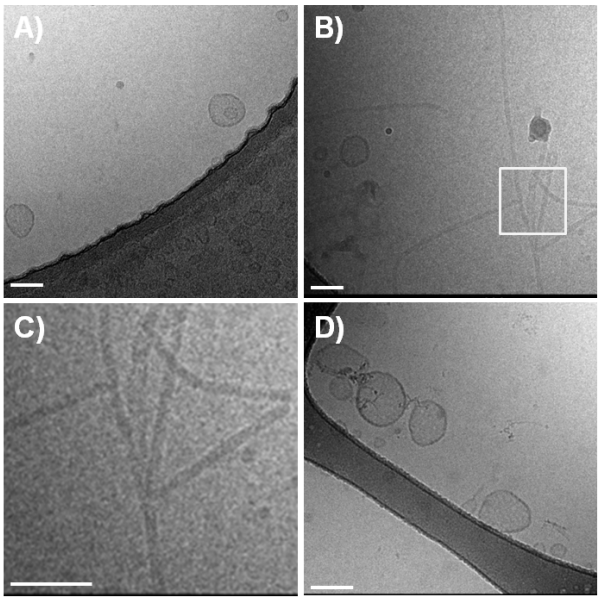

Figure 5. *Cryo-TEM images of the **CDV** + peptide **(1)** assembly. (A) 1 mM **CDV**s + 50 mol% peptide **1** at pH 7.4. (B) 1mM **CDV**s + 50 mol% peptide **1** at pH 5.0. (C) Enlarged section of (B). (D) 1mM **CDV**s + 50 mol% peptide **1**, back at pH 7.4. The scale bar represents 100 nm.*

Next the change of morphology upon pH adjustment as a function of time was studied **(Figure 6)**. In order to observe this time dependent transition, the peptide concentration was lowered to 20%. At 50 mol% peptide, the transition to fibers is complete within 5 minutes. Here, images were obtained 15 minutes and 1 hour after acidification from pH 7.4 to 5.0. After 15 minutes of incubation the predominant morphology was deformed vesicles. The assemblies have at this point already lost their spherical shape; however they have not yet obtained the fiber-like structure. After 1 hour, the deformed vesicles were no longer present and elongated vesicles and fiber-like structures were observed.

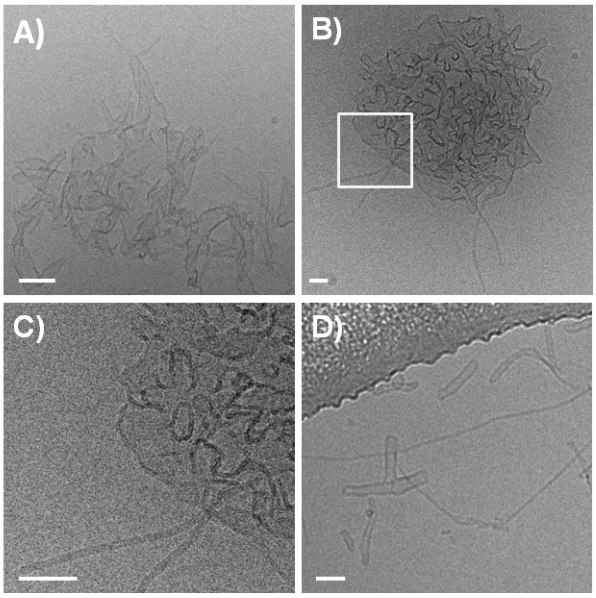

Figure 6. *Cryo-TEM images acquired from a sample containing 1mM CDVs and 20 mol% peptide **1**. (A) and (B): 15 minutes after acidification and (C) Magnified area of (B) (D): 60 minutes after acidification. The scale bar represents 100 nm.*

The final investigation concerning peptide **(1)** was conducted to show the difference in morphology that is associated with different peptide concentrations **(Figure 7)**. With a low peptide concentration mostly elongated vesicles are observed where at elevated peptide concentrations predominantly fibers are noted and the amount of fibers increased with increasing peptide concentration. These findings indicate a concentration dependence of the fiber formation based on the additional forces during the β-sheet formation of the peptides on the CDVs.

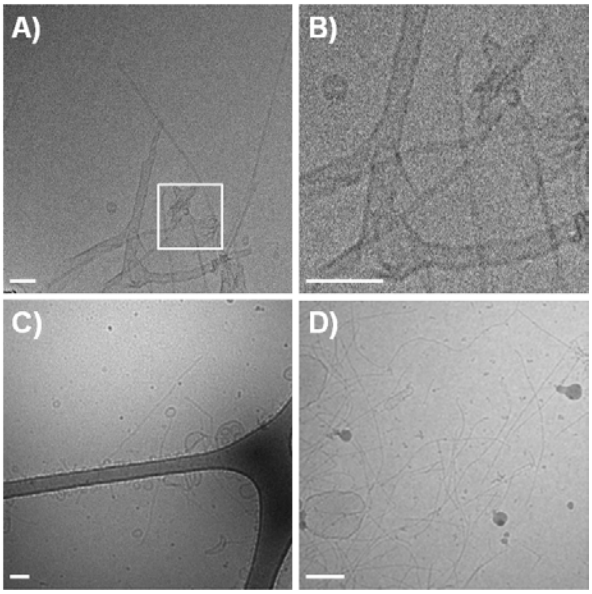

Figure 7. *Cryo-TEM images of 1mM CDVs with different concentrations of peptide **(1),** (A) 20 mol%, (B) Magnified area of picture (A), (C) 50 mol% and (D) 100 mol% at pH 5.0, 1 hour after acidification. The scale bar represents 100 nm.*

CDVs + peptide (2)

Assemblies formed by peptide conjugate **(2)** and cyclodextrin vesicles were investigated. Contrary to peptide **(1)**, peptide **(2)** affected the structural integrity of the CDVs at pH 7.4 **(Appendix, Figure S2)**. At low pH large fibers were observed which were present as bundles **(Figure 8 A-C)** and not as single fibers as obtained from peptide **(1)**. The single fibers were around 10 nm thick and several hundred nm long. The flexibility of the introduced spacer increases the freedom of movement of the octapeptides and extends them further from the CDV surface. It is possible that peptides located on a CDV are able to interact with peptides located on a neighbouring CDV, which would account for the observation that the fibers tend to stick to each other. Upon raising the pH to 7.4 again, the aggregated fibers were dissolved, which is consistent with the CD data, which showed that the β-sheet domains were formed reversibly. However, the original morphology was not obtained, as the amphiphilic cyclodextrin was present in flat sheets.

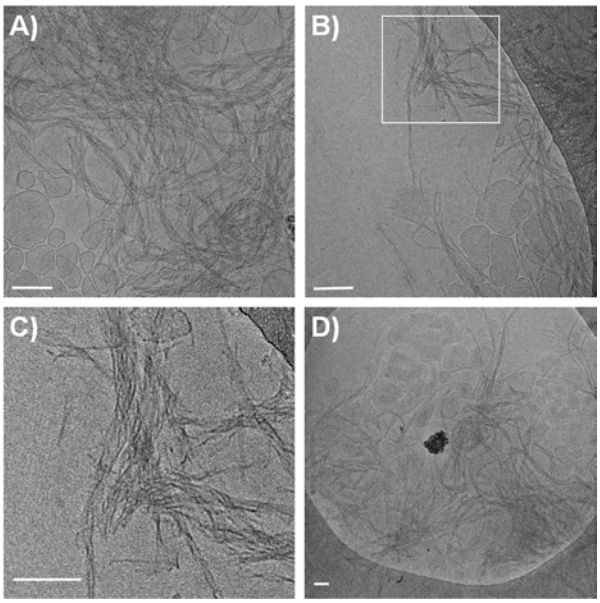

Figure 8. *Cryo-TEM images acquired of the assembly CDV (1 mM) + 50 mol% peptide* ***(2).*** *Images A), B) and C) were collected 1 hour after acidification. Image D) was collected after raising the pH again to 7.4 Picture C) represents the magnified area of picture B) The scale bar represents 100 nm.*

CDV + peptide (3)

The interaction of peptide **(3)** at pH 7.2 with the cyclodextrin vesicles leads to a complete disruption of the vesicular structures due to the strong binding of peptide **(3)** with the cyclodextrins, most likely this is due to the divalent interaction of the hydrophobic adamantane functionalities with the CD-cavities. Cryo-TEM images of the formed structures reveal short worm-like structures and some less well-defined assemblies **(Figure 9)**. The rod-like structures have a length of only 5-10 nm. A high contrast was observed, indicating a high density of organic material. This is in agreement with micellar structures without the existence of an aqueous compartment. Upon lowering the pH to 5.6, a transition from short worm like structures to fibers and tubular structures were observed, showing lengths up to several hundred nanometers.

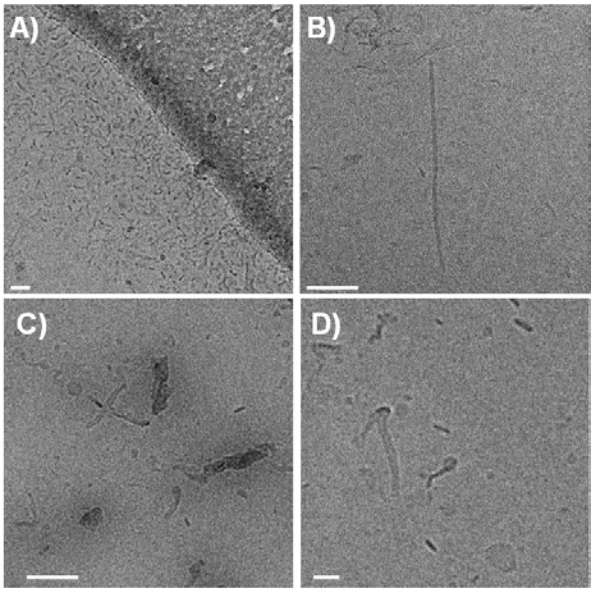

Figure 9. *Cryo-TEM images acquired of the assembly CDV (1 mM) + peptide **3.** A) pH = 7.2 and B), C), D) pH = 5.2**,** The images were collected with 50 mol% peptide **(3)**, 1 hour after adding the peptide. The scale bar represents 100 nm.*

All of the morphological transitions on display in this contribution are summarized in **Table 2**. When added to CDVs, both peptide **(1)** and peptide **(2)** give spherical assemblies, although the latter does affect the structural integrity of the membrane of the assembly. Addition of peptide **(3)** caused the assemblies to take on the shape of wormlike micelles. By lowering the pH, fibers (peptide **(1)**), aggregated fibers (peptide **(2)**), and wormlike micelles (peptide **(3)**) were observed. Only in the case of peptide **(1)**, were the pH driven morphological transitions reversible.

Table 2. *Summary of the observed morphological transitions and reversibility.*

Peptide	CDVs at pH 7.3	CDVs ~ pH 5	Reversibility
(1)	Spherical vesicles	Fibers	+
(2)	Spherical vesicles	Aggregated fibers	-
(3)	Wormlike micelles	Wormlike micelles	-

To study whether amphiphilic exchange between discrete assemblies occurs in the transition from vesicles to fibers (for peptide **(1)** and **(2)**), a lipid mixing assay was

performed. For this purpose, the amphiphilic cyclodextrin was fluorescently labeled with rhodamine B **(4)** according to a literature procedure **(Figure 10)**.[36]

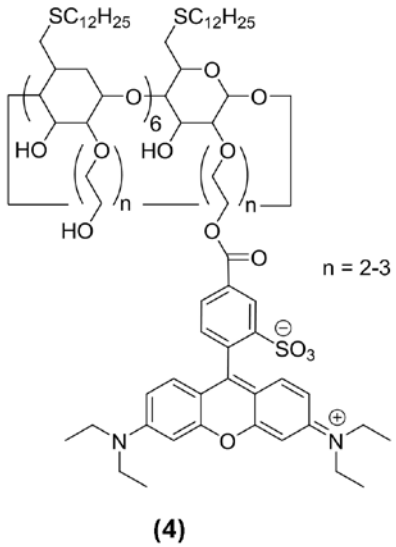

(4)

Figure 10. *Chemical structure of fluorescently labeled amphiphilic β-cyclodextrin.*

The amount of amphiphilic cyclodextrins that contained a fluorescent label was determined to be 4.6% by a Lambert Beer plot. These labeled cyclodextrins are also able to form vesicles in aqueous media. Due to the close proximity of the rhodamine B units at the vesicle surface a significant quenching is observed. These fluorescent vesicles were mixed with non-fluorescent CDVs in a ratio of 1:5 in the presence of either guest **(1)** or **(2)**. If during the pH dependent transformation between vesicles and fibers several vesicles take part, a significant increase in the rhodamine B distance should be the consequence of mixing of labeled and non labeled vesicles. With this a relief of self quenching and an increase of rhodamine B fluorescence should be observed. From **Figure S3** and **S4** in the appendix it is clearly visible that the addition of the guest molecules **(1)** and **(2)** to the CDVs and changing the pH does not lead to an increase in the emission intensity at 590 nm. Therefore, the assay reveals that no amphiphilic cyclodextrin mixing occurs between CDVs. In conclusion, in every morphological change a single vesicle is involved and not an interaction of multiple assemblies.

Controlled release of the CDV + peptide (1) assembly

So far it was observed that the *β*-sheet formation of the peptide strands is caused by a rearrangement of the peptide strands to adopt the optimal distance for the formation of hydrogen bonds. As the peptides are noncovalently bound to CDVs, the bilayer membrane of the vesicles and hence the entire assembly is affected by *β*-sheet formation, causing the transition of vesicles to single fibers when peptide **(1)** was used**.** The interior volume of the CDV-peptide **(1)** assemblies decreases significantly upon fiber formation and it could therefore act as a potential pH-responsive delivery system. The assemblies containing peptides **(2)** and **(3)** were not viable candidates as drug delivery systems, since the vesicles were unable to encapsulate cargo without significant leakage. Therefore, uptake and release of the fluorescent dye tetrasodium 1,3,6,8-pyrene tetrasulfonate (Py) from CDV-peptide **(1)** was studied. These vesicles were prepared in the presence of the dye and subsequently, NaI was added to quench the fluorescent activity of non-encapsulated dye. No significant leakage was observed for the assembly with peptide **(1)**. After the pH was lowered to 5.0, a significant decrease in fluorescent intensity was observed, which was caused by Py molecules being released from the assembly **(Figure 10)**. The pH range in which the release takes place is of interest as this range is also found in living cells, where the high pH corresponds to the for example the extracellular medium and the low pH corresponds to endosomes. A drug delivery system based on CDV- peptide **(1)** might therefore be able release its cargo inside endosomes. Subsequent endosomal escape results in delivery of the cargo to the cytoplasm.

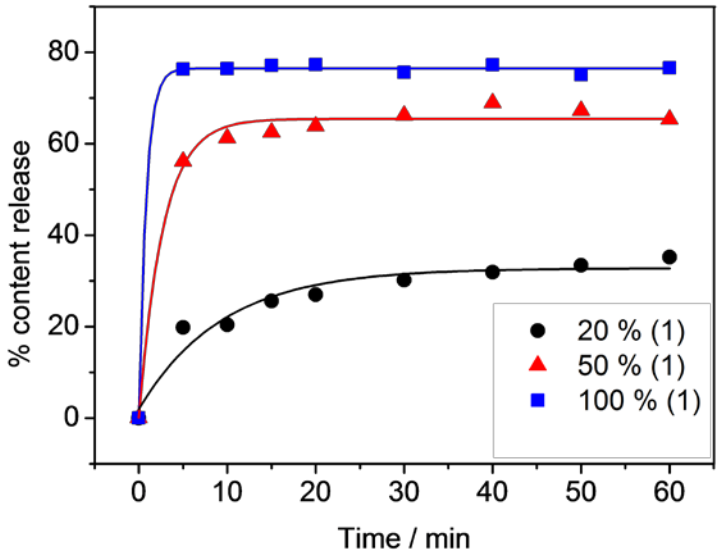

Figure 11. *Time dependent release profiles of Py for the assembly CDV-peptide **(1)** with 0.5 mM CDV and various peptide concentrations at ~pH 5.*

At low peptide **(1)** concentrations (20 mol%) a steady release was observed and about 30% of the cargo was released from the CDV-peptide **(1)** assembly. At higher peptide concentrations (50 and 100 mol%) around 70% and 80% of the fluorescent dye was released. This data was consistent with the cryo-TEM data, as it was observed that the cause of content release, the extent of fiber formation, was also dependent on the peptide concentration. This shows that the CDV-peptide **(1)** assembly can be used as a pH sensitive delivery system, of which the release profile can be adjusted as a function of the peptide concentration.

Conclusions

Stimulus responsive supramolecular assemblies consisting of CDVs and adamantane modified oligopeptides have been constructed. The system features the careful orchestration of several orthogonal non-covalent interactions. The dense packing of peptide strands at the surface of the CDVs allows for the formation of β-sheet domains at low pH and the formation of these highly ordered structures was found to be reversible. Upon β-sheet formation, the assembly with peptide **(1)** formed fiber like structures and with peptide **(2)** the fibers aggregated into bundles. Upon addition of peptide **(3)**, the morphology of the assembly was found to change into wormlike

micelles. It was shown that the fiber formation for the assembly CDV-peptide **(1)** caused the assembly to release a high percentage of the encapsulated cargo and that the released amount could be adjusted as a function of the peptide concentration. Therefore, this supramolecular system can be of use as a pH sensitive delivery system and a nanoscale switching device.

References

1. E. Krieg and B. Rybtchinski, *Chem.-Eur. J.*, 2011, 17, 9016-9026.
2. I. W. Hamley, V. Castelletto, C. Moulton, D. Myatt, G. Siligardi, C. L. P. Oliveira, J. S. Pedersen, I. Abutbul and D. Danino, *Macromol. Biosci.*, 2010, 10, 40-48.
3. B. E. McKenzie, F. Nudelman, P. H. H. Bomans, S. J. Holder and N. Sommerdijk, *J. Am. Chem. Soc.*, 2010, 132, 10256-10259.
4. S. Chiruvolu, S. Walker, J. Israelachvili, F. J. Schmitt, D. Leckband and J. A. Zasadzinski, *Science*, 1994, 264, 1753-1756.
5. C. Schmuck and W. Wienand, *Angew. Chem.-Int. Edit.*, 2001, 40, 4363-+.
6. S. Trier, J. R. Henriksen and T. L. Andresen, *Soft Matter*, 2011, 7, 9027-9034.
7. B. J. Ravoo, J. C. Jacquier and G. Wenz, *Angew. Chem.-Int. Edit.*, 2003, 42, 2066-2070.
8. V. Marchi-Artzner, M. J. Brienne, T. Gulik-Krzywicki, J. C. Dedieu and J. M. Lehn, *Chem.-Eur. J.*, 2004, 10, 2342-2350.
9. K. J. Lee, D. K. Lee, Y. W. Kim, W. S. Choe and J. H. Kim, *J. Polym. Sci. Pt. B-Polym. Phys.*, 2007, 45, 2232-2238.
10. F. Versluis, H. R. Marsden and A. Kros, *Chem. Soc. Rev.*, 2010, 39, 3434-3444.
11. S. Cavalli, F. Albericio and A. Kros, *Chem. Soc. Rev.*, 2010, 39, 241-263.
12. H. R. Marsden and A. Kros, *Angew. Chem.-Int. Edit.*, 2010, 49, 2988-3005.
13. N. C. Bellocq, D. W. Kang, X. H. Wang, G. S. Jensen, S. H. Pun, T. Schluep, M. L. Zepeda and M. E. Davis, *Bioconjugate Chem.*, 2004, 15, 1201-1211.
14. K. Peng, I. Tomatsu, A. V. Korobko and A. Kros, *Soft Matter*, 2010, 6, 85-87.
15. K. Peng, I. Tomatsu, B. van den Broek, C. Cui, A. V. Korobko, J. van Noort, A. H. Meijer, H. P. Spaink and A. Kros, *Soft Matter*, 2011, 7, 4881-4887.
16. M. Eddaoudi, J. Kim, N. Rosi, D. Vodak, J. Wachter, M. O'Keeffe and O. M. Yaghi, *Science*, 2002, 295, 469-472.
17. K. Wang, D. S. Guo, X. Wang and Y. Liu, *ACS Nano*, 2011, 5, 2880-2894.
18. C. M. Paleos, Z. Sideratou and D. Tsiourvas, *ChemBioChem*, 2001, 2, 305-310.
19. J. D. Hartgerink, E. Beniash and S. I. Stupp, *Science*, 2001, 294, 1684-1688.
20. S. Khan, S. Sur, C. J. Newcomb, E. A. Appelt and S. I. Stupp, *Acta Biomater.*, 2012, 8, 1685-1692.
21. S. Sur, E. T. Pashuck, M. O. Guler, M. Ito, S. I. Stupp and T. Launey, *Biomaterials*, 2012, 33, 545-555.
22. P. Besenius, Y. Goedegebure, M. Driesse, M. Koay, P. H. H. Bomans, A. R. A. Palmans, P. Y. W. Dankers and E. W. Meijer, *Soft Matter*, 2011, 7, 7980-7983.
23. D. C. Drummond, C. O. Noble, M. E. Hayes, J. W. Park and D. B. Kirpotin, *J. Pharm. Sci.*, 2008, 97, 4696-4740.
24. G. D. Bothun, *Journal of nanobiotechnology*, 2008, 6, 13.
25. X. Wang, E. J. Danoff, N. A. Sinkov, J. H. Lee, S. R. Raghavan and D. S. English, *Langmuir*, 2006, 22, 6461-6464.
26. J. Park, L. H. Rader, G. B. Thomas, E. J. Danoff, D. S. English and P. DeShong, *Soft Matter*, 2008, 4, 1916-1921.
27. M. Ueda, A. Makino, T. Imai, J. Sugiyama and S. Kimura, *Soft Matter*, 2011, 7, 4143-4146.
28. G. Battaglia and A. J. Ryan, *J. Am. Chem. Soc.*, 2005, 127, 8757-8764.

29. H. R. Marsden, C. B. Quer, E. Y. Sanchez, L. Gabrielli, W. Jiskoot and A. Kros, *Biomacromolecules*, 2010, 11, 833-838.
30. B. J. Ravoo and R. Darcy, *Angew. Chem.-Int. Edit.*, 2000, 39, 4324-4326.
31. M. R. Caira and D. R. Dodds, *Journal of Inclusion Phenomena and Macrocyclic Chemistry*, 2000, 38, 75-84.
32. M. E. Davis, *Molecular Pharmaceutics*, 2009, 6, 659-668.
33. M. D. Yilmaz, S. H. Hsu, D. N. Reinhoudt, A. H. Velders and J. Huskens, *Angew. Chem.-Int. Edit.*, 2010, 49, 5938-5941.
34. K. Tanaka and F. Toda, *Chem. Rev.*, 2000, 100, 1025-1074.
35. B. L. Zhang and R. Breslow, *J. Am. Chem. Soc.*, 1993, 115, 9353-9354.
36. J. Voskuhl, T. Fenske, M. C. A. Stuart, B. Wibbeling, C. Schmuck and B. J. Ravoo, *Chem.-Eur. J.*, 2010, 16, 8300-8306.
37. F. Versluis, I. Tomatsu, S. Kehr, C. Fregonese, A. Tepper, M. C. A. Stuart, B. J. Ravoo, R. I. Koning and A. Kros, *J. Am. Chem. Soc.*, 2009, 131, 13186-13187.
38. J. Voskuhl, M. C. A. Stuart and B. J. Ravoo, *Chem.-Eur. J.*, 2010, 16, 2790-2796.
39. S. K. M. Nalluri and B. J. Ravoo, *Angew. Chem.-Int. Edit.*, 2010, 49, 5371-5374.
40. S. K. M. Nalluri, J. Voskuhl, J. B. Bultema, E. J. Boekema and B. J. Ravoo, *Angew. Chem.-Int. Edit.*, 2011, 50, 9747-9751.
41. I. Kuzmenko, H. Rapaport, K. Kjaer, J. Als-Nielsen, I. Weissbuch, M. Lahav and L. Leiserowitz, *Chem. Rev.*, 2001, 101, 1659-1696.
42. E. T. Mack, P. W. Snyder, R. Perez-Castillejos, B. Bilgicer, D. T. Moustakas, M. J. Butte and G. M. Whitesides, *J. Am. Chem. Soc.*, 2012, 134, 333-345.
43. B. F. Shaw, G. F. Schneider, H. Arthanari, M. Narovlyansky, D. Moustakas, A. Durazo, G. Wagner and G. M. Whitesides, *J. Am. Chem. Soc.*, 2011, 133, 17681-17695.
44. J. Huskens, A. Mulder, T. Auletta, C. A. Nijhuis, M. J. W. Ludden and D. N. Reinhoudt, *J. Am. Chem. Soc.*, 2004, 126, 6784-6797.

Experimental section

General synthesis procedures

All reactions were carried out under an argon atmosphere (Argon 4.8 from *Fa. Messer-Griesheim*) using flasks which were flame-dried under vacuum. Dry septa, disposable syringes and needles were used for the transfer of solvents and chemicals. The air- and water-free solvents were obtained by refluxing with suitable reagents and distillation under an argon atmosphere. Preparative flash column chromatography was performed under 1 bar argon pressure using silica gel grade 40–63 μm purchased from MERCK, Darmstadt. Solvents for column chromatography were distilled prior to us. Thin layer chromatography was done using commercially available aluminium silica gel cards 60 F 254 purchase from MERCK, Darmstadt. The detection of the products was done under UV light at 254 nm Exact mass spectral measurements were carried out on Micro Tof (Bruer Daltronics, Bremen). Calibrations were done directly before the measurements of samples with sodium formate-clusters.

The ^{1}H and ^{13}C NMR spectra were recorded at ARX 300 and AMX 400 spectrometer (from BRUKER ANALYTISCHE MESSECHNIK, Karlsruhe). All measurements were carried out in $CDCl_3$ [δ ^{1}H ($CHCl_3$) = 7.24;^{13}C ($CDCl_3$) = 77.0 (1:1:1 t)]. TMS [δ ^{1}H (TMS) = 0.0;^{13}C (TMS) = 0.0] was used as internal standard for calibrating the NMR spectra. The signals are described as s: singlet, dd: doublet of doublet, m: multiplet. The assignment of the resonances were proved by two dimensional homonuclear and heteronuclear correlation experiments such as ^{1}H-^{1}H-COSY (GCOSY), ^{13}C-^{1}H-GHSQC, or ^{13}C-^{1}H-GHMBC experiments. With respect to a better comparison of the spectroscopic data the numbering does not follow IUPAC nomenclature.

Synthesis of the adamantane modified peptides

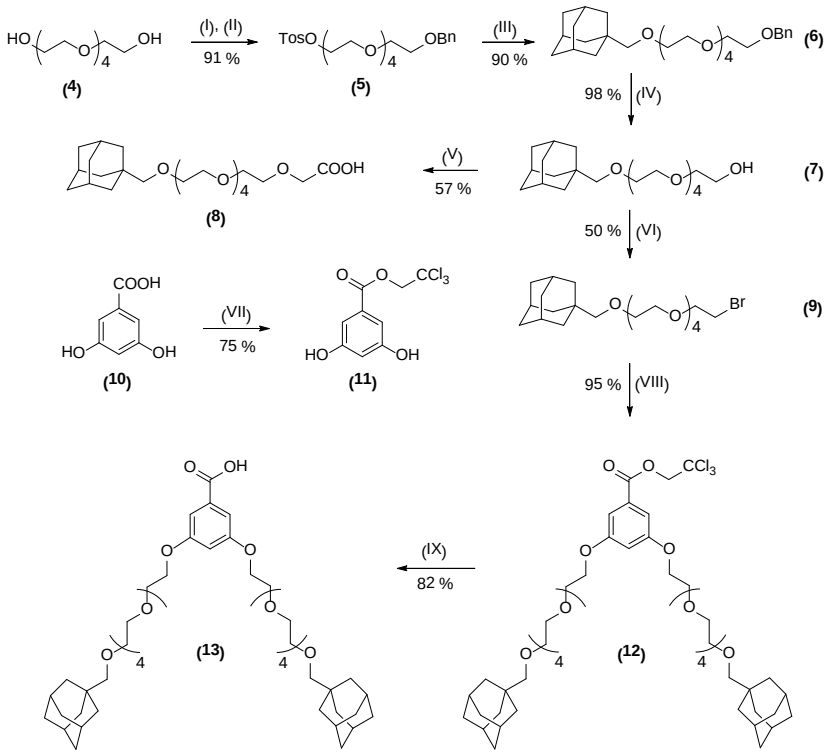

Scheme S1: Reaction pathway to the adamantane anchors **(8)** and **(13)**. **(I)** BnBr, NaOH, THF, 24 h, 100 °C, **(II)** TosCl, NEt_3, DMAP, CH_2Cl_2, rt, 2h, **(III)** Adamantanemethanol, NaH, DMF, 24 h, rt, **(IV)** Pd/C, MeOH, H_2, 20 h, rt, **(V)** Bromoacetic acid, *t*-BuOK, DMF, 130°C rt, **(VI)** PBr_3, toluene, 24h, rt, **(VII)** Trichloroethanol, H_2SO_4, 70 °C, 5 d, **(VIII)** K_2CO_3, **(11)**, CH_3CN, 70°C, 3d, **(IX)** Zinc dust, acetic acid, THF, 2 h, rt.

<u>Synthesis of toluene-4-sulfonic acid 2-[45] -ethyl ester (5):</u>

(I) A solution of NaOH (1.00 g, 25 mmol) in DMF (15 ml) was added to a mixture of tetraethylene glycol **1** (20 g, 100 mmol) and benzyl bromide (2.34 g, 25 mmol). The reaction mixture was stirred at 100 ^{o}C for 24 h. The reaction mixture was cooled, extracted with CH_2Cl_2 (3 x 50 ml) and the organic extracts were combined. Drying of the organic layer with $MgSO_4$, and evaporation of the solvent under reduced pressure afforded (6.74 g, 95% yield) product **2**. ^{1}H NMR (400 MHz, $CDCl_3$, 25°C, TMS): δ=7.30 (s, 5H; =CH^{Bn}), 4.48 (s, 2H; OCH$_2$^{Bn}), 3.65–3.31 (m, 16H; OCH_2CH_2O) ppm; ^{13}C NMR (100 MHz, $CDCl_3$, 25°C, TMS): δ=138.3 (C_q, *ipso*-C^{Bn}), 128.4, 128.1, 127.6 (CH, =CH^{Bn}), 72.5 (CH_2, OCH$_2$^{Bn}), 70.6, 70.5, 69.9, 69.4 (CH_2, OCH_2CH_2O [without assignment]), 61.5 (CH_2, CH_2OH) ppm; IR: $\tilde{\nu}$=3390, 3290, 2870, 1103 cm^{-1}; Exact mass for $C_{15}H_{24}O_5Na$: *m/z* calcd: 307.1516; found: 307.1520 $[M + Na]^+$.

(II) NEt_3 (3.20 g, 32 mmol) was added dropwise to a solution of **2** (6.00 g, 20 mmol) and DMAP (0.08 g) in CH_2Cl_2 (5 mL) at 0°C and stirred at 0°C for 5 minutes. Subsequently, *p*-toluenesulfonyl chloride (4.00 g, 20 mmol) was added slowly and the reaction mixture was stirred for 3 h at room temperature. Then the reaction mixture was extracted with Et_2O (3 × 20 mL). The combined organic phases were dried over anhydrous $MgSO_4$ and concentrated in vacuo. The residue was purified by flash column chromatography on silica gel (petroleum ether : EtOAc = 2:1, R_f = 0.37) to give **3** (8.90 g, 96% yield). ^{1}H NMR (400 MHz, $CDCl_3$, 25°C, TMS): δ=7.5 (dd, ^3J(H,H)=8.3Hz, ^3J(H,H)=3.7Hz, 4H; $=CH^{Tos}$), 7.26 (s, 5H; $=CH^{Bn}$), 4.0 (dd, ^2J(H,H)=5.9Hz, ^2J(H,H)=4.8Hz, 2H; $OCH_2{}^{Bn}$), 3.61–3.48 (m, 16H; OCH_2CH_2O), 2.36 (s, 3H; CH_3) ppm; ^{13}C NMR (100 MHz, $CDCl_3$, 25°C, TMS): δ=144.7 (C_q, *ipso*-C^{Tos}), 138.2 (C_q, *ipso*-C^{Bn}), 133.0 (C_q, *ipso*-C^{Tos}), 129.8, 128.3 (CH, $=CH^{Tos}$), 127.9, 127.6, 127.4, (CH, $=CH^{Bn}$), 73.2 (CH_2, $OCH_2{}^{Bn}$), 70.7, 70.6, 70.5, 69.4 (CH_2, OCH_2CH_2O), 21.6 (CH_3, CH_3) ppm; IR: $\tilde{\nu}$=2868, 1598, 1496 cm^{-1}; Exact mass for $C_{22}H_{30}O_7SNa$: *m/z* calcd: 461.1634; found: 461.1611 $[M + Na]^+$.

Synthesis of 1-(2-{2-[2-(2-Benzyloxy-ethoxy)-ethoxy]-ethoxy}-ethoxymethyl)-adamantane (6):

A suspension of sodium hydride (1.00 g, 40 mmol) in DMF (2 ml) was added slowly to a solution of 1-adamantanmethanol (**4**) (3.32 g, 20 mmol) in DMF (15 ml) at 0°C, under argon atmosphere. The reaction mixture was stirred at room temperature for 90 min. The solution of **3** (8.80 g, 20 mmol) in DMF (5ml) was added to the reaction mixture. Subsequently, the reaction mixture was stirred at room temperature for 24 h. Then reaction mixture was extracted with CH_2Cl_2 (3 x 50 ml) and the organic extracts were combined. Drying of the organic layer with $MgSO_4$, evaporation of the solvent under reduced pressure and purification by flash column chromatography on silica gel (petroleum ether : EtOAc = 3:1, R_f = 0.65) afforded (7.76 g, 90% yield) product **5**. ^{1}H NMR (400 MHz, $CDCl_3$, 25°C, TMS): δ=7.26 (s, 5H; $=CH^{Bn}$), 4.49 (s, 2H; $OCH_2{}^{Bn}$), 3.58–3.46 (m, 16H; OCH_2CH_2O), 2.94 (s, 2H; $OCH_2{}^{Ad}$), 1.87 (m, 3H; 3-CH^{Ad}), 1.65 (m, 6H; 4-$CH_2{}^{Ad}$), 1.55 (m, 6H; 2-$CH_2{}^{Ad}$) ppm; ^{13}C NMR (100 MHz, $CDCl_3$, 25°C, TMS): δ=137.2 (C_q, *ipso*-C^{Bn}), 127.3, 127.1, 126.7 (CH, $=CH^{Bn}$), 108.7 (CH_2, $OCH_2{}^{Ad}$), 81.4 (CH_2, $OCH_2{}^{Bn}$), 75.2 (CH_2, $OCH_2{}^{Bn}$), 72.8, 72.2, 69.6, 69.6 (CH_2, OCH_2CH_2O), 38.6 (CH_2, 2-$CH_2{}^{Ad}$), 37.4 (CH_2, 4-$CH_2{}^{Ad}$), 33.4 (C_q, 1-C^{Ad}), 27.1

(CH, 3-CH^{Ad}) ppm; IR: $\tilde{\nu}$=2848, 1674, 1503, 1387 cm^{-1}; Exact mass for $C_{26}H_{40}O_5Na$: *m/z* calcd: 455.2768; found: 455.2766 $[M + Na]^+$.

Synthesis of 2-(2-{2-[2-(Adamantan-1-ylmethoxy)-ethoxy]-ethoxy}-ethoxy)-ethanol (7):

A suspension of catalytic amount of Pd/C (0.20 mg) and **5** (7.20 g, 16 mmol) in EtOH (40 ml) was stirred at room temperature under 2 bar H_2 atmosphere for 20 h. The suspension was filtrated and solvent was evaporated. Product **6** was used without further purification (5.60 g, 98% yield). ^{1}H NMR (300 MHz, $CDCl_3$, 25°C, TMS): δ=3.65–3.48 (m, 16H; OCH_2CH_2O), 2.94 (s, 2H; OCH_2^{Ad}), 1.88 (m, 3H; 3-CH^{Ad}), 1.62 (m, 6H; 4-CH_2^{Ad}), 1.45 (m, 6H; 2-CH_2^{Ad}) ppm; ^{13}C NMR (75 MHz, $CDCl_3$, 25°C, TMS): δ=82.9 (CH_2, OCH_2^{Ad}), 73.1, 71.1, 71.0, 70.8, (CH_2, OCH_2CH_2O), 62.1 (CH_2, CH_2OH), 40.1 (CH_2, 2-CH_2^{Ad}), 37.4(CH_2, 4-CH_2^{Ad}), 34.6 (C_q, 1-C^{Ad}), 28.7 (CH, 3-CH^{Ad}) ppm; IR: $\tilde{\nu}$=2844, 1642 cm^{-1}; Exact mass for $C_{19}H_{34}O_5Na$: *m/z* calcd: 365.2298; found: 365.2302 $[M + Na]^+$.

Synthesis of [2-(2-{2-[2-(Adamantan-1-ylmethoxy)-ethoxy]-ethoxy}-ethoxy)-ethoxy]-acetic acid (8):

A suspension of *t*BuOK (1.47 g, 12.90 mmol) in DMF (2 ml) was added slowly to a solution of **6** (1.50 g, 4.38 mmol) in DMF (15 ml) at 0°C, under argon atmosphere and the mixture was stirred at room temperature for 30 min. To this reaction mixture the solution of bromoacetic acid (1.20 g, 8.76 mmol) in DMF (1 ml) was added. The reaction mixture was stirred at 130°C for 15 h. Subsequently, the reaction mixture was extracted with CH_2Cl_2 (3 x 30 ml) and 2 M HCl. The organic extracts were combined, the organic layer was dried with $MgSO_4$. Evaporation of the solvent under reduced pressure and purification by flash column chromatography on silica gel (CH_2Cl_2 : MeOH = 5:1, R_f = 0.3) afforded (1.00 g, 58% yield) product **7**. ^{1}H NMR (400 MHz, $CDCl_3$, 25°C, TMS): δ=3.98 (s, 2H; OCH_2C=O), 3.63–3.45 (m, 16H; OCH_2CH_2O), 2.96 (s, 2H; OCH_2^{Ad}), 1.85 (m, 3H; 3-CH^{Ad}), 1.64 (m, 6H; 4-CH_2^{Ad}), 1.44 (m, 6H; 2-CH_2^{Ad}) ppm; ^{13}C NMR (100 MHz, $CDCl_3$, 25°C, TMS): δ=175.0 (C_q, C=O), 82.4 (CH_2, OCH_2^{Ad}), 71.1, 70.9, 70.6, 69.7, (CH_2, OCH_2CH_2O), 69.0 (CH_2, O*C*H_2C=O), 39.6 (CH_2, 2-CH_2^{Ad}), 37.2 (CH_2, 4-CH_2^{Ad}), 34.1 (C_q, 1-CAd), 28.2 (CH, 3-CH^{Ad}) ppm; IR: $\tilde{\nu}$=2856, 1594, 1448 cm^{-1}; Exact mass for $C_{21}H_{36}O_7Na$: *m/z* calcd: 423.2353; found: 423.2355 $[M + Na]^+$.

Synthesis of 1-(2-{2-[2-(2-Bromo-ethoxy)-ethoxy]-ethoxy}-ethoxymethyl)-adamantane (9):

PBr_3 (1.56 g, 5.84 mmol) was added dropwise to a solution of 7 (4.00 g, 12.00 mmol) in toluene (25 mL) at 0^oC and reaction mixture was stirred at 0^oC for 30 minutes. Then reaction mixture was stirred for 15 h at room temperature. Subsequently, the mixture was extracted with CH_2Cl_2 (3 × 50 mL). The combined organic phases were dried over anhydrous $MgSO_4$ and concentrated in vacuo. The residue was purified by flash column chromatography on silica gel (CH_2Cl_2 : MeOH = 99:1, R_f = 0.8) to give 9 (2.36 g, 50% yield). ^1H NMR (400 MHz, $CDCl_3$, 25°C, TMS): δ=3.66–3.42 (m, 16H; OCH_2CH_2O), 2.86 (s, 2H; OCH_2^{Ad}), 1.83 (m, 3H; 3-CH^{Ad}), 1.54 (m, 6H; 4-CH_2^{Ad}), 1.32 (m, 6H; 2-CH_2^{Ad}) ppm; ^{13}C NMR (100 MHz, $CDCl_3$, 25°C, TMS): δ=82.4 (CH_2, OCH_2^{Ad}), 71.2, 70.7, 70.6, 70.5, (CH_2, OCH_2CH_2O), 39.6 (CH_2, 2-CH_2^{Ad}), 37.3 (CH_2, 4-CH_2^{Ad}), 33.8 (C_q, 1-C^{Ad}), 28.2 (CH, 3-CH^{Ad}) ppm; IR: $\tilde{\nu}$=2957, 1633, 1450 cm^{-1}; Exact mass for $C_{19}H_{33}O_4BrNa$: *m/z* calcd: 427.1436; found: 427.1460 $[M + Na]^+$.

Synthesis of 3,5-Dihydroxy-benzoic acid 2,2,2-trichloro-ethyl ester (11):

To a solution of 2,2,2-trichloroethanol (30 ml) was added 3,5-dihydroxybenzoic acid (5.00 g, 32.50 mmol) followed by concentrated sulphuric acid (1 ml), and the mixture was heated at 70^oC for 5 days under argon atmosphere. The reaction mixture was extracted with CH_2Cl_2 (3 × 50 mL). The combined organic phases were dried over anhydrous $MgSO_4$ and concentrated in vacuo. The residue was purified by flash column chromatography on silica gel (CH_2Cl_2 : EtOAc = 1:5) to give **10** (6.60 g, 75% yield). ^1H NMR (400 MHz, $CDCl_3$, 25°C, TMS): δ=7.08 (s, 2H; =CH^{Ph}), 6.57 (s, 1H; =CH^{Ph}), 4.83 (s, 2H; OCH_2CCl_3) ppm; ^{13}C NMR (100 MHz, $CDCl_3$, 25°C, TMS): δ=163.3, (C_q, C=O), 156.9 (C_q, C^{Ph}), 130.4 (C_q, C^{Ph}), 109.6 (CH, =CH^{Ph}), 108.7 (CH, =CH^{Ph}), 99.2 (C_q, CCl_3), 74.7 (CH_2, O*C*H_2CCl_3) ppm; Exact mass for $C_9H_7O_4Cl3Na$: *m/z* calcd: 306.9302; found: 306.9290 $[M + Na]^+$.

Synthesis of 3,5-Bis-[2-(2-{2-[2-(adamantan-1-ylmethoxy)-ethoxy]-ethoxy}-ethoxy)-ethoxy]-benzoic acid 2,2,2-trichloro-ethyl ester (12):

The reaction mixture of **10** (0.67 g, 2.46 mmol) and K_2CO_3 in CH_3CN (100 ml) was heated at 70°C. Subsequently, the mixture of KI (0.50 g, 0.71 mmol) and **8** (2.00 g, 4.0 mmol) in CH_3CN (10 ml) was added slowly to the reaction mixture. The final reaction mixture was heated at 80°C for 72 h. Then reaction mixture was extracted with CH_2Cl_2 (3 x 30 ml) and 2 M HCl. The organic extracts were combined and the organic layer was dried with $MgSO_4$. Evaporation of the solvent under reduced pressure and purification by flash column chromatography on silica gel (CH_2Cl_2 : MeOH = 9:1, R_f = 0.87) afforded **12** (2.20 g, 95% yield). ^{1}H NMR (400 MHz, $CDCl_3$, 25°C, TMS): δ=7.25 (s, 2H; =CH_{ortho}), 6.73 (s, 1H; =CH_{meta}), 4.92 (s, 2H; OCH_2CCl_3), 4.13 (m, 2H; $C_{ipso}OCH_2CH_2O$), 3.67–3.43 (m, 14H; OCH_2CH_2O), 2.89 (s, 2H; OCH_2^{Ad}), 1.89 (m, 3H; 3-CH^{Ad}), 1.62 (m, 6H; 4-CH_2^{Ad}), 1.49 (m, 6H; 2-CH_2^{Ad}) ppm; ^{13}C NMR (100 MHz, $CDCl_3$, 25°C, TMS): δ=164.5 (C_q, C=O), 159.8 (C_q, $C_{ipso}O$), 130.3 (C_q, $C_{ipso}C$=O), 108.5 (CH, =CH_{ortho}), 107.3 (CH, =CH_{meta}), 94.9 (C_q, CCl_3), 82.5 (CH_2, OCH_2^{Ad}), 74.4 (CH_2, OCH_2CCl_3), 71.9, 71.7, 70.6, 70.5, (CH_2, OCH_2CH_2O), 39.6 (CH_2, 2-CH_2^{Ad}), 37.1 (CH_2, 4-CH_2^{Ad}), 34.0 (C_q, 1-C^{Ad}), 28.2 (CH, 3-CH^{Ad}) ppm; IR: $\tilde{\nu}$=2848, 1735, 1592, 1446 cm^{-1}; Exact mass for $C_{47}H_{71}Cl_3O_{12}Na$: *m/z* calcd: 955.3887; found: 957.3846 $[M + Na]^+$.

Synthesis of 3,5-Bis-[2-(2-{2-[2-(adamantan-1-ylmethoxy)-ethoxy]-ethoxy}-ethoxy)-ethoxy]-benzoic acid (13):

Acetic acid (4.5 ml) was added to a solution of **12** (1.70 g, 1.82 mmol) in THF (40 ml) and the reaction mixture was stirred at room temperature under argon atmosphere. Subsequently, zinc dust (0.78 g) was added, and the mixture was stirred vigorously at room temperature for 1 h. The reaction mixture was filtered, and the filtrate was extracted with Et_2O (3 x 50 ml). The combined extracts were washed with water and dried over $MgSO_4$. The solvent was removed and the crude product was purified by flash column chromatography on silica gel (CH_2Cl_2 : MeOH = 7:1, R_f = 0.88) and product **13** (1.20 g, 82% yield) was obtained as an oil. ^{1}H NMR (400 MHz, $CDCl_3$, 25°C, TMS): δ=7.20 (s, 2H; =CH_{ortho}), 6.69 (s, 1H; =CH_{meta}), 4.13 (m, 2H; $C_{ipso}OCH_2CH_2O$), 4.11 (m, 2H; $C_{ipso}OCH_2CH_2O$), 3.69–3.45 (m, 12H; OCH_2CH_2O), 2.89 (s, 2H; OCH_2^{Ad}), 1.92 (m, 3H; 3-CH^{Ad}), 1.69 (m, 6H; 4-CH_2^{Ad}),

1.50 (m, 6H; 2-CH_2^{Ad}) ppm; ^{13}C NMR (100 MHz, $CDCl_3$, 25°C, TMS): δ=170.2 (C_q, C=O), 159.7 (C_q, $C_{ipso}O$), 131.7 (C_q, $C_{ipso}C$=O), 108.4 (CH, $=CH_{ortho}$), 107.3 (CH, $=CH_{meta}$), 82.5 (CH_2, OCH_2^{Ad}), 71.3, 71.1, 70.8, 70.6, (CH_2, OCH_2CH_2O), 39.7 (CH_2, 2-CH_2^{Ad}), 37.1 (CH_2, 4-CH_2^{Ad}), 34.0 (C_q, 1-C^{Ad}), 28.2 (CH, 3-CH^{Ad}) ppm; IR: $\tilde{\nu}$=2848, 1716, 1592, 1446 cm^{-1}; Exact mass for $C_{45}H_{70}O_{12}Na$: *m/z* calcd: 825.4759; found: 825.4748 $[M + Na]^+$.

Solid phase peptide synthesis of (1), (2) and (3)

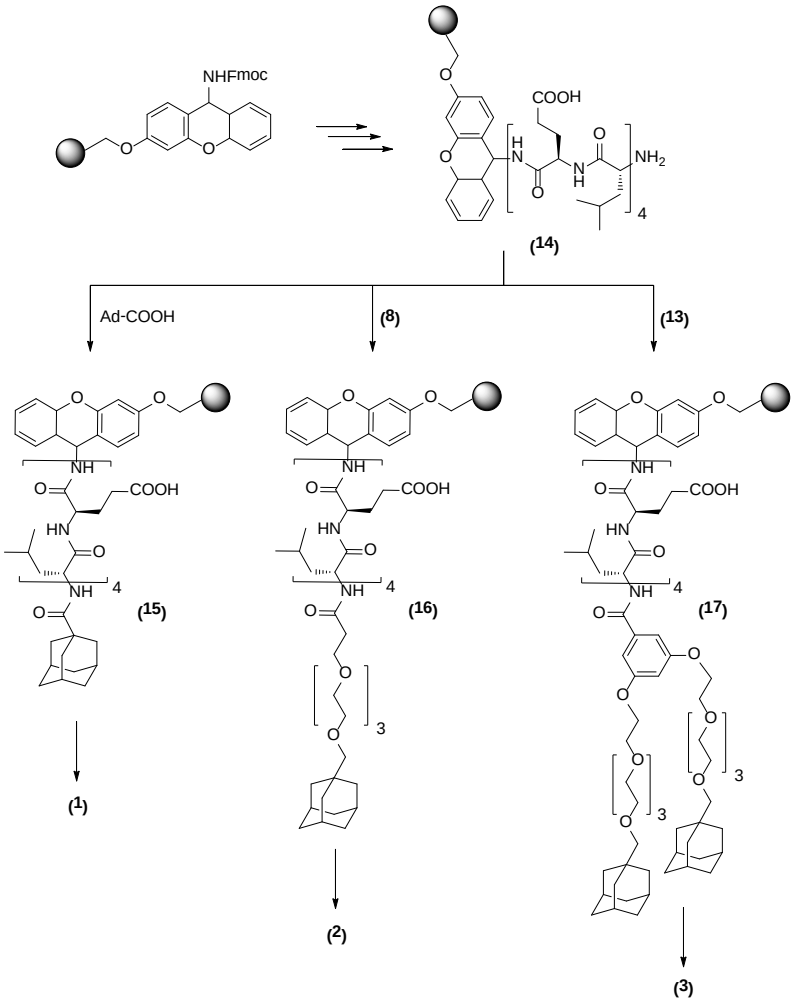

Scheme S2: Reaction pathway to the adamantane modified peptides **(1)**, **(2)** and **(3)**.

<u>Fmoc-NH-(leu-glu)$_4$-NH-resin (14)</u>

The octapeptide was synthesized using a conventional Fmoc solid phase peptide synthesis protocol on an Applied Biosystems 431A automated peptide synthesizer. The peptide was synthesized on a Sieber amide resin with a loading of 0.64 mmol/g at

a 250 μmol scale. Amino acid couplings were performed in NMP for 1 hour with 4 equivalents of HCTU, 8 equivalents of base and 4 equivalents of the appropriate amino acid. Fmoc deprotection was performed with 20 vol% piperidine in NMP.

Ad-(leu-glu)$_4$-NH-resin (15)

The octapeptide (**14**) was conjugated to adamantane by coupling adamantane 1-carboxylic acid to the N-terminus of the peptide. The resin was swollen in NMP for 1 hour. A mixture of 4 eq. adamantane 1-carboxylic acid, 4 eq. of HCTU and 8 eq. of DIPEA in NMP was left to activate for 2 minutes after which it was added to the resin and coupled overnight.

Ad-TEG$_4$-(leu-glu)$_4$-NH-resin (16)

The octapeptide (**14**) was conjugated to **8** by coupling it to the N-terminus of the peptide. The resin was swollen in NMP for 1 hour. A mixture of 4 eq. of **13**, 4 eq. of HCTU and 8 eq. of DIPEA in NMP was left to activate for 2 minutes after which it was added to the resin and coupled overnight.

(Ad-TEG$_4$)$_2$-Phe-(leu-glu)$_4$-NH-resin (17)

The octapeptide (**14**) was conjugated to **13** by coupling it to the N-terminus of the peptide. The resin was swollen in NMP for 1 hour. A mixture of 4 eq. of **13**, 4 eq. of HCTU and 8 eq. of DIPEA in NMP was left to activate for 2 minutes after which it was added to the resin and coupled overnight.

Cleavage and purification of (15), (16) and (17)

Products **(1)**, **(2)** and **(3)** were obtained by cleaving the corresponding molecules from the resin by treating them with a solution containing TFA:H_2O (9:1 v/v). The solutions with the products were co-evaporated with toluene 3 times to obtain the dry crude product. Subsequent RP-HPLC was performed on a Shimazu HPLC system with two LC-8A pumps and an SPD-10AVP UV-VIS detector. Two different eluents were used: (A) H_2O (with 0.1% TFA) and (B) CH_3CN (with 0.1% TFA). The flow rate was 20 mL/min. The gradient was set to 10%-90% B over 3 column volumes. Collection of the product peak was determined by UV absorption at 214 nm. The acetonitril was removed through rotary evaporation and subsequent lyophilization

yielded the pure products in powder form. The purity of compounds **(1)**, **(2)** and **(3)** was determined by LCMS, and was estimated to be greater than 95%.

General characterization procedures

Preparation of the cyclodextrin-vesicles

Amphiphilic *β*-cyclodextrin **1** was synthesized as described.[2] To prepare unilamellar bilayer vesicles, **1** was dissolved in CHCl3 and the solvent was evaporated with a rotary evaporator and a vacuum oven for one hour. The obtained thin film of **1** was hydrated with phosphate buffered saline and was vortexed extensively at room temperature (PBS, pH 7.4) to provide a 1 mM turbid aqueous solution of **1**. After sonication under heating for 30 minutes, a clear solution was obtained. The size of the vesicles was set around 100 nm by extrusion through a polycarbonate membrane. The average diameter of the particles was estimated to be 77 nm with dynamic light scattering.

***β*-Sheet formation on the surface of the CD vesicle**

After the appropriate amount of peptide **2** (typically 0.5 mM solution in PBS) was added to vesicles composed of **1** (typically 0.5 mM solution in PBS), the pH of the mixture was set to 5.0 with a minimum amount of a 0.1 M H3PO4 or 1 M HCl.

Circular dichroism (CD) spectroscopy

CD spectra were measured with a J-815 Spectropolarimeter (JASCO) at room temperature. A 0.1 cm quartz cuvette was used. The CD spectra were obtained after averaging of six scans and subtraction of the background. The molar ellipicity, [θ] (deg cm2 dmol-1), was calculated from the observed ellipticity, θ*obs* (mdeg), by applying the following equation: $[\theta] = \theta obs \cdot M/(10 \cdot l \cdot c)$, where *M* is the mean residue molecular weight, *l* is the path length of the cuvette in cm and *c* is the concentration of the peptide in mg/mL.

Dynamic Light Scattering (DLS)

DLS data were obtained using a Zetasizer Nano ZS (Malvern Instruments Ltd). The observed intensity autocorrelation function, $g(2)(t)$, was measured experimentally, which is related to the normalized autocorrelation function, $g(1)(t)$, by the Siegert

relation, $g(2)(t) = 1 + \beta \cdot [g(1)(t)]2$, where β is a constant parameter for an optical system. To obtain the average relaxation time (τ), the first cumulant method was employed to analyze $g(1)(t)$ according to the equation, $g(1)(t) = \exp(-t/\tau)$. The apparent translational diffusion coefficient, D, is calculated from $D = \Gamma\_/q2$, where Γ is the relaxation rate, $\Gamma = 1/\tau$, and q represents the magnitude of scattering vector expressed as $q = (4\pi n/\lambda\square) \cdot \sin(\theta/2)$, where θ is the scattering angle, 173°, n is the refractive index of the solution and λ is the wavelength (633 nm). The apparent hydrodynamic radius, r, is given by the Einstein-Stokes equation $r = kBT/(6\pi\eta D)$, where kB is the Boltzmann constant, T is the absolute temperature, and η is the solvent viscosity.

Cryo-TEM

Glow-discharged carbon-coated lacey Formvar grids (300 mesh, Ted Pella) or Quantifoil R2/2 grids (Quantifoil, Jena Germany) were loaded with 3 μL sample. Grids were blotted and plunged into liquid ethane using a fully automated home-built vitrification device operating at 100 % humidity and 22 ºC. Electron microscopy images were recorded on a FEI Tecnai 12 electron microscope at an accelerating voltage of 120 keV and equipped with a 4k x 4k Eagle camera (FEI, Eindhoven, The Netherlands). Images were recorded at liquid nitrogen temperature using a Gatan 626 cryo-holder (Gatan Inc., Pleasanton, U.S.A.) under low-dose conditions.

Fluorescence Spectroscopy

Fluorescence measurements were performed using a FS920 fluorometer (Edinburgh Instruments Ltd.) with a DTMS-300X excitation monochrometer and a peltier-controlled thermostatic cell. All spectra were obtained at 25 °C using a quartz cuvette with a 1 cm path length. Each spectrum was measured with the step size of 1.0 nm, and a sampling time of 0.1 s, and single scan. Excitation and emission slits were 1 nm. The excitation wavelength was 282 nm. For the fluorescence experiment a 10 μM solution of tetrasodium 1,3,6,8-pyrenetetrasulfonate and 100 mM of NaI was used. To destroy the assembly, a minimum amount of 20 wt% Triton X-100 solution was used. The experiment was performed as follows: tetrasodium 1,3,6,8-pyrenetetrasulfonate (Py) was added during the preparation of the vesicular system composed of **1** and **2**. Next, NaI was added to quench all non-encapsulated dyes, the observed signal was

due only to encapsulated dyes. The pH was then lowered to 5.0 with 1 M HCl and the fluorescence intensity was measured for 1 hour. Triton X-100 was then added and the fluorescence intensity was measured again.

Isothermal Titration Calorimetry (ITC)

ITC titrations were performed with a Nano-ITC III (Calorimetry Sciences Corporation, USA). The reference cell was filled with Milli-Q grade water. All solutions were degassed for 10 min before use. The guest molecules (5.00 mM for **(2)**, and 2.50 mM for **(3)**) were dissolved in water with addition of 1 equivalent of NaOMe to increase the water solubility. 20 injections with a volume of 10μL were titrated into a solution of β-CD (0.5 mM) in milli-Q water. Injection intervals were set to 300 seconds with a stirring rate of 300 rpm and a temperature of 23°C.

Appendix: Supplementary information

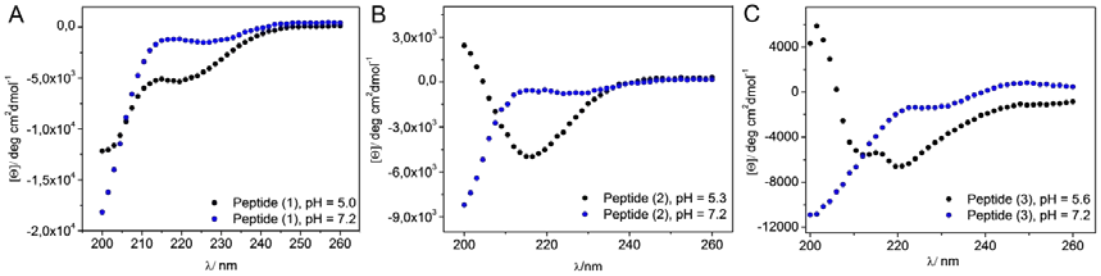

Figure S1. CD spectra of **(1)**, **(2)** and **(3)** at pH = 7.2 (black) and pH = ~5 (blue).

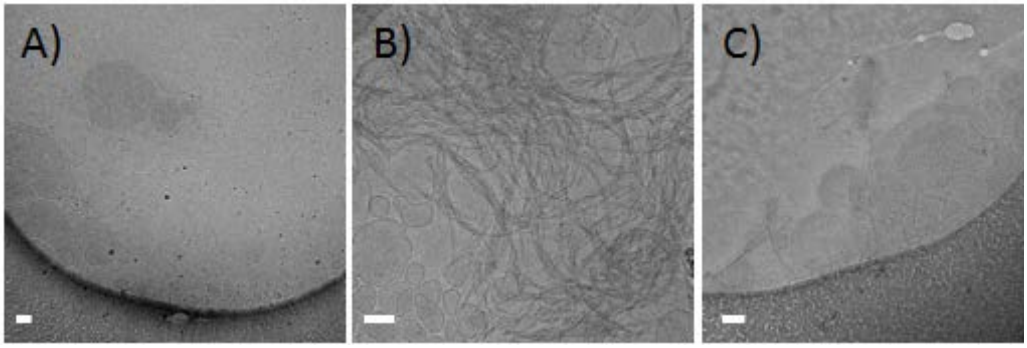

Figure S2. Cryo-TEM images acquired of the assembly CDV + peptide **(2)** at A) pH 7.4, B) pH 5.3 and C) back to pH 7.4.

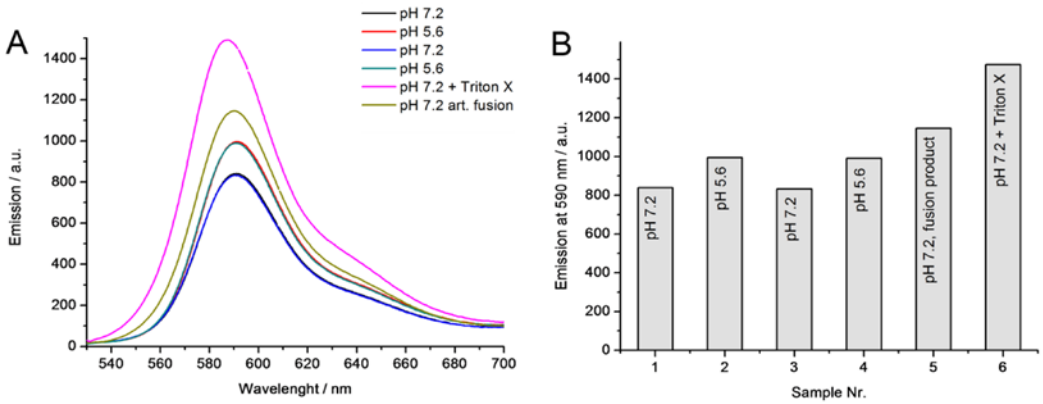

Figure S3. Lipid mixing assay of **(1)** with β-CD vesicles. Emission spectra (left) and max. emission at 590 nm (right).

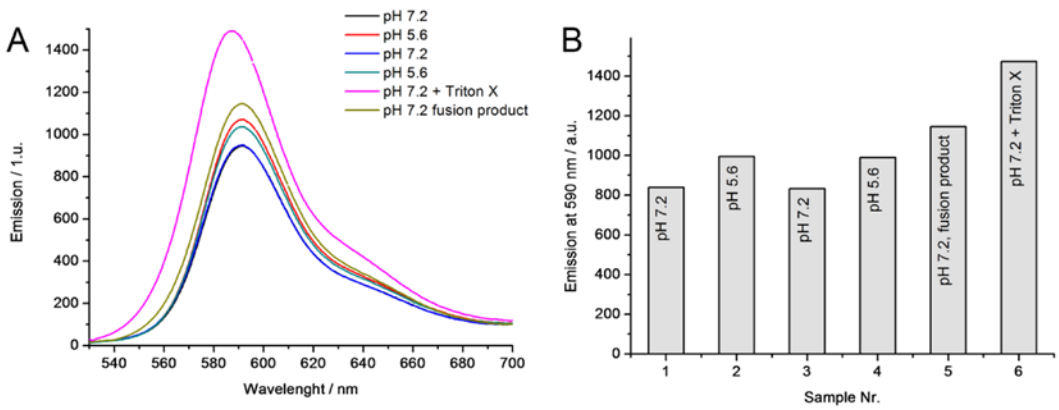

Figure S4. Lipid mixing assay of **(2)** with β-CD vesicles. Emisson spectra (left) and max. emissions at 590 nm (right).